Military Technical College
Kobry El-Kobbah,
Cairo, Egypt.

18th International Conference on Applied Mechanics and Mechanical Engineering.

EFFECT OF ELECTRON BEAM WELDING PARAMETERS ON DISSIMILAR JOINTS OF AISI 430 FERRITIC STAINLESS STEEL AND AISI 1020 LOW CARBON STEEL

M. Nasr El-Deen*, M. E. Shamekh*, W. Elthalabawy* and M.T. Sallam*

ABSTRACT

This paper presents the optimization of welding parameters of electron beam welded joint of dissimilar materials namely AISI 430 ferritic stainless steel and AISI 1020 low carbon steel (0.21% C.). Three main welding parameters were investigated. These parameters are welding current, focusing current and welding speed. The optimization was based, from one hand, on microstructure analysis of both bead and heat affected zones, using optical and scanning electron microscopes, and, from the other hand, the evaluation of tensile, impact, and micro-hardness mechanical properties. The results of the investigation showed that, an optimum welding current of 24 mA, a focusing current of 875 mA, and a welding speed of 8mm/s at a working distance 100 mm can provide uniform welding bead with full penetration, without undercuts and a narrow width of HAZ. Moreover, they can secure a tensile failure outside the joint, in the base metal (low carbon steel) satisfying a tensile strength of about 431 MPa. Furthermore, the impact resistance of the joint was found to provide about 160 J/cm^2 (hammer against the root of bead) and about 60 J/cm^2 (hammer against the face of bead). The hardness distribution along the joint from the stainless steel side to the low carbon steel side through the bead and HAZ was determined, and indicates that, a maximum hardness of about 380 HV was obtained in the center of the bead. This value is higher than the obtained hardness values of both the ferritic stainless steel and low carbon steel.

KEYWORDS

HAZ: Heat Affected Zone, **EBW:** Electron Beam Welding

* Egyptian Armed Forces.

INTRODUCTION

Several situations in industrial practice face challenges which call for joining of dissimilar materials [1,2]. The joining of dissimilar metals is generally more complex than that of similar metals because of the difference in the physical, mechanical, and metallurgical properties of both parent metals to be joined [3,4]. Aerospace vehicles and nuclear reactors are examples of the most important applications among many others. In nuclear water reactors, dissimilar metal welds are employed to connect the low alloy steel reactor pressure vessel and stainless steel pipe systems [1,3, 5].

The essential problem with the dissimilar metal weld made between low alloy steel and ferritic stainless steel is the carbide formation due to higher carbon content of low alloy steels than that of ferritic stainless steel [6,7]. Many techniques used to weld dissimilar metals such as shielded metal arc welding, gas metal arc welding, tungsten arc welding, plasma arc welding [3,4,5], laser beam welding, and electron beam welding [3,8].

In most of these critical applications, electron beam welding technique is considered the best candidate and is used. In electron beam welding, the heat input is concentrated on the interface and melts the metal (Keyhole phenomena) [8]. Many parameters control this process like welding current, focusing current, welding speed, sweep size, and working distance between the gun and work piece [8,9].

Arivazhagan et al. [10] studied the investigation on 304 stainless steel to 4140 low alloy steel dissimilar joints by gas tungsten arc, friction welding, and electron beam welding. The analysis showed that the joint made by EBW has the highest tensile strength than the joint made by GTAW and FRW. He also found that the ductility of the EBW and GTA weldment were higher compared with friction weldment.

I. Hajiannia [11], Investigated the microstructure and mechanical properties of AISI 347 stainless steel to ASTM A335 low alloy steel dissimilar joint by using TIG with two filler metals including ER309L and ERNiCr-3. The tensile test analysis showed that all weldments failed in the HAZ of A335 low alloy steel.

ZHANG Bing-gang, [12] studied the temperature and stress fields in electron beam welded Ti-15-3 alloy to 304 stainless steel joint with copper interlayer sheet. He concluded that the temperature distribution is asymmetric along the weld center and the temperature in the titanium alloy plate is higher than that in the 304 stainless steel plate.

In this paper, three major electron beam welding parameters were optimized and investigated. These parameters control the magnitude of the heat input delivered to the joint during the welding process [13,14]. The optimization of these parameters was based on the evaluation of the obtained microstructure and mechanical properties of the elaborated joints [15].

EXPERIMENTAL WORK

The base metals employed in this study are ferritic stainless steel (AISI 430) and low carbon steel (AISI 1020). These base metals were both delivered in the form of rolled

plates 5 mm thickness. Composition analysis had been determined by using X-Ray florescence and Spark emission spectroscopy. The chemical compositions of both metals are shown in Table 1.

The metals were cut into similar plates with dimensions 100x80x5 mm by using laser machine model (TruLaser 3030) as shown in Fig.1

Several different plates were welded by electron beam welding technique without edge preparation and air gap under constant accelerating voltage of 60 KV, vacuum pressure of 26x10-3 Pa and working distance of 100 mm, using an EBW machine model (SeoTECH-60) shown in Fig. 2.

Three major welding parameters were chosen to be investigated, and each has been varied independently while keeping the other parameters to be constant. Welding current, as a welding parameter, has the major effect on the value of the energy input and the resulting characteristic of the welded joint. This welding current was changed during this investigation from 9 mA up to 29 mA. Outside these range, joining was difficult to take place. On the other hand, the focusing current, which is considered as the second basic welding parameter, having a notable effect on controlling the position of the beam spot along the thickness of the plate, concentrates the input energy in the vertical position. By increasing the focusing current, the beam spot shifts down from the surface, through the thickness, to the root of the joint. Focusing current was varied from 865 mA to 885 mA to secure the required depth of beam spot. The welding speed, which also considerably affects the value of the energy input, during the weld, was varied from 3mm/s up to 13mm/s. A working distance of 100 mm was kept constant during carrying out of all experimental joints.

Standard tensile test specimens, having the welded bead, in the middle, perpendicular to the longitudinal axis of the specimen, were cut from the welded plates according to ASTM E8. These specimens have a gauge length of 80 mm and a gauge area of 20x5mm. Tensile test was carried out on these specimens according to ASTM E8/E8M-13 under strain rate of 10-3 s-1, using a universal tensile electro-hydraulic testing machine type Instron 8032.

Furthermore, non-standardize non-notched impact specimens having dimensions 55x10x5mm were also cut, so that, the weld bead is located in the middle of the specimen length. Impact test was carried out, on each specimen, in two directions, hummer against face and hummer against root of the weld, by using automatic impact testing machine type Galdabini 300.

Hardness test, was carried out, applying the Vickers's hardness test method, according to ISO 17025, using Zwick hardness tester applying indentation load of 1 Kg. HV values were recorded along a line perpendicular to the weld bead from the side of the ferritic stainless steel through HAZ and bead toward the low carbon steel side.

Specimens for microstructure were prepared applying the standard procedure, after mounting in polyethylene holders, grinding with emery papers of varies grades 180, 250, 400, 600, 800, and 1200,was carried out, followed by polishing using an emulsion of AL2O3 in distilled water, to have a mirror like surface. Revealing of the structure was carried out using two types of etchants, due to the different sensitivity

of reaction of both structures for a single etchant. Etching was first applied by immersion in Nital reagent (3% NHO3 - methyl alcohol) for 10s to reveal the low carbon steel structure. Afterward, Villa's etchant (5cc HCL + 2gr Picric acid + 100cc Ethyl alcohol) was applied for 1 min. to reveal the ferritic and bead structure. Low carbon steel structure after applying this second etchant was severely over etched and becomes extremely dark. The different microstructures were examined by an optical microscope type Olympus BX41M.

RESULTS AND DISCUSSIONS

Microstructure Analysis

The obtained microstructures of the base metals are illustrated in Fig. 3. The structure of the AISI 430 ferritic steel Fig. 3a indicates that, it is fully ferrite with clear deformed grains oriented in the rolling direction. On the contrary, the structure of the low carbon steel AISI 1020 Fig. 3b reveals a mixture of pearlite and a dominant ferritic phase. We can note also the deformation and elongation of the grains in the direction of the previous rolling operations.

The evolution of the structure from the bead towards the base metal through the transition boundary and heat affected zone (HAZ), of dissimilar welded joint between the adopted ferritic stainless steel and low carbon steel, is demonstrated in Fig. 4. This joint was elaborated by applying a welding current of Iw=24 mA, focusing current of If=875mA, and a welding speed of v=8mm/s. The investigation of the microstructure in the bead region clearly reveals the existence of columnar dendritic grains oriented towards the center of the bead. Closely adjacent to the interface region on AISI 430 steel side, we can recognize a clear zone of coarse equiaxed grains followed by another zone subjected to recrystallization and carbide precipitations, while, on the other side, closely adjacent to the interface region on AISI 1020 steel side, we can identify very narrow zone of average equiaxed grains followed by deformed un-affected grains of the base metal of the original plate. This can also be explained by the difference of thermal conductivity between the two plates which is higher in the low carbon steel than ferritic stainless steel.

Mechanical Testing Results

Figure 5 illustrates typical Stress-Strain curves obtained during testing welded dissimilar joints of ferritic stainless steel and low carbon steel, by different welding current Iw with constant focusing current of If=875 mA and welding speed of v=8mm/s. When a welding current of 9 mA was applied, the obtained joint strength and strain were very moderate. Increasing the welding current up to 14 mA, the ultimate strength showed a slight increase. This indicates that the heat input supplied to the joint by this range of welding current is not enough to guarantee uniform and homogeneous welding bead. When the welding current was increased to 19 mA, strength and particularly strain were remarkably increased. Further increase of welding current, up to 24 mA, enhances the joint strength but reduces the joint ductility. For higher values of welding current, both strength and ductility start to decrease again.

Figure 6 shows the variation of the obtained joint ultimate tensile strength with the applied welding currents, under constant focusing current of 875 mA and welding speed of 8 mm/s. It can be noted that a maximum ultimate tensile strength of 431 MPa was achieved using a welding current of 24 mA. The measured values of ductility as a function of welding current indicate that a maximum joint ductility of 20 % can be obtained by using a welding current of 19 mA, as shown in Fig. 7. Hence, when the strength is of prime joint concern, a welding current of 24 mA is recommended, while 19 mA is endorsed when the joint ductility is of high consideration. This effect can be directly attributed to the eminent differences in the welded materials compositions, micro-constituents, and physical, thermal, and mechanical properties.

Figure 8 shows the variation of the characteristics of typical stress-strain curve, of welded dissimilar joints of ferritic stainless steel and low carbon steel by changing the welding speed, at an optimum welding current of Iw=24 mA and focusing current of If=875 mA. It can be noted that, when the welding speed was very low (3 mm/s), the joint stress strain curve demonstrated enough high ductility and showed a pronounced yield point which is an intrinsic behavior of low carbon steel. On the other hand, the maximum strength was lower than that of both types of the used plates. This is also consolidated by the occurrence of fracture in the bead zone. When the welding speed was increased up to (8 mm/s), the obtained joint stress strain diagram demonstrated the maximum ultimate tensile strength on the expense of considerable reduction of ductility. Furthermore, when the welding speed was extensively increased (13 mm/s), the heat input was seriously reduced and consequently, the joint quality extremely degraded. The joint stress strain diagram, in this case, demonstrates humble strength and very limited ductility.

Figure 9 summarizes the variation of the joint ultimate tensile strength as a function of welding speed and shows that a welding speed of 8 mm/s can provide a maximum ultimate tensile strength of 431 MPa. On the contrary, the ductility showed a monotonic decrease with increasing the welding speed as illustrated in Fig. 10. Also the optimum value of welding speed can be correlated to the applications and requirements on the elaborated joint as indicated before, when the welding of dissimilar materials of ferritic stainless steel and low carbon steel, was considered. When strength is the major concern, then a welding speed of 8mm/s can provide an optimum value, while, when ductility is of prime importance, then the low value of welding speed v=3mm/s can be establish.

Figure 11 presents the effect of changing the focusing current on the resulting stress-strain curves of dissimilar joints of ferritic stainless steel and low carbon steel under a constant welding current of Iw= 24 mA and a welding speed of v= 8 mm/s. The investigation of the effect of the focusing current, which controls the position of the electron beam spot through the thickness of the specimen from the top surface to the bottom root, showed a similar behavior of the obtained mechanical properties as those measured during varying the welding speed. By increasing the focusing current, ultimate tensile strength increases up to a maximum value of 431 MPa at a focusing current of 875 mA where further increase of the focusing current leads to decrease this strength, as shown in Fig. 12. Moreover, by increasing the focusing current, the ductility monotonically decreases, as illustrated in Fig. 13. The optimum value of the focusing current can also be determined on the same bases as welding speed.

The results of the measured impact toughness on the electron beam dissimilar joints, of ferritic stainless steel and low carbon steel, as a function of welding current, under a constant focusing current of 875 mA and a welding speed of 8 mm/s, are demonstrated in Fig. 14. The impact toughness was measured in two directions, hammer against the root of bead and hammer against the face of bead. When hammer strikes against the face of the bead, the root serves as a notch, in joints with partial or bad penetration. On the contrary, when hammer strikes against the root of the bead, the joint performs as non-notched impact specimen. This can explain the higher values of the impact toughness obtained when the hammer strikes against the root of the bead (non-notched impact specimen). On the other hand, the maximum values of impact toughness, in both directions of hammer strikes relative to the bead, are about 79 J and 28.6 J respectively, under a welding current of Iw=19 mA.

The effects of welding speed and focusing current on impact toughness, keeping the other welding parameters constant, are illustrated in Fig. 15 and Fig. 16. We can note that the determined optimum focusing current and welding speed from the analysis of the results of the tensile tests can also provide maximum values of impact toughness.

Figure 17 shows the hardness distribution, along a line, from the stainless steel side of the welded plates, through the heat affected zones and formed bead, to the low carbon steel side of the joint. The measured values of hardness for the initial plates are in the order of 210 HV for AISI 430 ferritic stainless steel and 135 HV for AISI 1020 low carbon steel. In the center of the bead, a clear peak of hardness can be noticed, its amplitude increases with increasing the value of welding current up to 24 mA where it attains 387 HV. For higher values of welding current, the amplitude of this peak starts to decrease again. On the contrary, we are no longer being able to visualize the drop of hardness observed in other similar and dissimilar joints, in the HAZ. This can be explained by the recovery and recrystallization processes that take place in these regions which are subjected to temperature lower than the transformation temperatures but higher than the recrystallization one. Actually these processes of recovery and recrystallization take place in these zones but their effect is masked by an adverse effect of formation of strong single and complex carbides of chromium which has a remarkable influence on increasing the hardness in the bead and HAZ. In fact, according to the compositions of the indicated steels, through the joint, there will be establish important diffusion gradients, from one hand, for chromium from the stainless steel side to the low carbon steel side and, from the other hand, for carbon in the opposite direction. It was found that the coefficient of diffusion of chromium in ferritic stainless steel with nearly absence of nickel is much more important than the same coefficient of diffusion in the austenitic stainless steels with considerable existence of nickel.

CONCLUSION

1. Welding current and welding speed are considered the predominant welding parameters controlling the heat input to the welded joint and consequently the obtained structure and joint quality after solidification of the bead.
2. The optimum welding parameters, for welding dissimilar joints of AISI 430 ferritic stainless steel and AISI 1020 low carbon steel plates, having 5 mm thickness,

are Iw=24 mA, If=875 mA, and v=8 mm/s. These parameters secure the highest strength, while Iw=19 mA secures the highest ductility and toughness.

3. Ductility of these welded joints monotonically decreases by increasing both welding speed and focusing current.
4. Higher values of the impact toughness obtained when the hammer strikes against the root of the bead, where the joint acts as non-notched impact specimen. When hammer strikes against the face of the bead, the values of toughness is reduced to about half of the corresponding values obtained when hammer strikes against the face of the bead. The maximum values of impact toughness, in both directions of hammer strike relative to the bead were obtained at an optimum welding current of Iw=19 mA.
5. A peak of hardness was obtained in the center of the bead due to the diffusion process and formation of single and complex carbides. Hardness drops, in both sides of the joint, through the HAZ. Some regions in HAZ were subjected to softening by the recrystallization effect of the initial deformed plates structure.

REFERENCES

[1] Sindo Kou, ”Welding metallurgy”, Wiley, 2003.
[2] O.P. Khanna, “Welding Technology”, Dhanpat Rai Publications Ltd., 2006.
[3] W. Robbert, Jr. Messler, “Joining of Materials and Structures”, ELSEVIER, 2003.
[4] R.S. Parmar, “Welding engineering and technology”, New Delhi: Khanna Publishers, 2003.
[5] David Leroy Olson, “Welding, Brazing, and Soldering”, Vol.6, ASM international, 1993.
[6] J. R. Davis, “Stainless Steels”, ASM International, Materials Park, Ohio, 1996.
[7] C. John, Lippold, and J. Kotecki Damian” Welding Metallurgy and Weldability of Stainless Steel”, Wiley, 2005.
[8] N. Yilbas, A.F.M. Arif, B.J. Abdul Aleem,” Laser welding of low carbon steel and thermal stress analysis”, Optics & Laser Technology, 42, (760–768), 2010.
[9] S. P. Tewari, “Effect of welding parameters on the weldability of material”, Inter. Jour. of Eng. Sci. and Tech., India vol. 2(4), (512-516), 2010.
[10] N. Arivazhagan, Surendra Singh, Satya Prakash, G.M. Reddy,” Investigation on AISI 304 austenitic stainless steel to AISI 4140 low alloy steel dissimilar joints by gas tungsten arc, electron beam and friction welding”, Mat. and Design, 32, (3036-3050), 2011.
[11] I. Hajiannia, M. Shamanian, M. Kasiri, “Microstructure and mechanical properties of AISI 347 stainless steel/A335 low alloy steel dissimilar joint produced by gas tungsten arc welding”, Mat. and Design, 50, (566-573), 2013.
[12] Zhang Bing-gang, Wang Ting, Dyan Xiao-hui, “Temperature and stress fields in electron beam welded Ti-15-3 alloy to 304 stainless steel joint with copper interlayer sheet”, Trans. Nonferrous Met. Soc., China 22,(398-403), 2012.
[13] L. Grecu, G. Demian,” The Influence of welding parameters on temperature distribution in case of EBW”, DAAAM inter. Scien. Book, 5, (035-044), 2009
[14] Subodh Kumar, A.S. Shahi,” Effect of heat input on the microstructure and mechanical properties of gas tungsten arc welded AISI 304 stainless steel joints”, Mat. and Design, 32, (3617-3623), 2011.

[15] Jun Yan, MingGao , Xiaoyan Zeng, " Study on microstructure and mechanical properties of 304 stainless steel joints by TIG, laser, and laser-TIG hybrid welding", Optics and Lasers in Eng., 48, (512–517), 2010.
[16] C. Meola and A. Squillace," Analysis of stainless steel welded joints: a comparison between destructive and non destructive techniques", Journal of Mat. Processing Tech., 155–156, (1893–1899), 2004.
[17] S. Murugan and S. K. Rai, "Temperature distribution and residual stress due to multi-pass welding in type 304 stainless steel and low carbon steel weld pads", Inter. Jour. of pressure vessels and piping, 78, (307-317), 2001.
[18] T. Mohandas, G. Madhusudan Reddy and B. Satish Kumar," Heat-affected zone softening in high-strength low-alloy steels", Jour. of Mat. Processing Tech., Vol. 88, (284-294), 1999.
[19] M. G. Ananth and B. S. Babu," Experimental Investigations on Electron Beam Welding of Austenetic /Ferritic Stainless Steel for Space Applications", Inter. Jour. of Research in Mech. Eng. & Tech., IJRMET, Vol. 3, 2013.
[20] A. Służalec," Theory of Thermo-mechanical Processes in Welding", Springer, 2005.
[21] Schultz, Electron Beam Welding. UK: Abington Puplishing 2004.
[22] J. C. H. S.H. WU, and Y.N. WANG, "Evolution of Microstructure and Texture in Mg-Al-Zn Alloys during Electron-Beam and Gas Tungsten Arc Welding", Metallurgical and Materials Transactions, vol. 35 A, pp. 2455-2469, 2004.
[23] Y. I. Sazonov, "Problems of Engineering Diagnostics of Electron beam welding", Russian journal of Non-Destructive Testing, vol. 42, pp. 823-836, 2006.
[24] A. S. S. Subodh Kumar, "Effect of heat input on the microstructure and mechanical properties of gas tungsten arc welded AISI 304 stainless steel Joints", Mat. and Design, vol. 32, pp. 3617-3623, 2011.
[25] M. S. K. U.S.Patil, "Effect of the welding process parameter in MMAW for joining of dissimilar metals and parameter optimization using artificial neural fuzzy interface system", Inter. Journal of Mechanical Eng. and Technology, vol. 4, pp. 6340-6359, 2013.

Fig. 1. The Laser Machine type (TruLaser 3030) used in cutting plates and test specimens.

Fig. 2. The Chamber of the used Electron Beam Welding Machine.

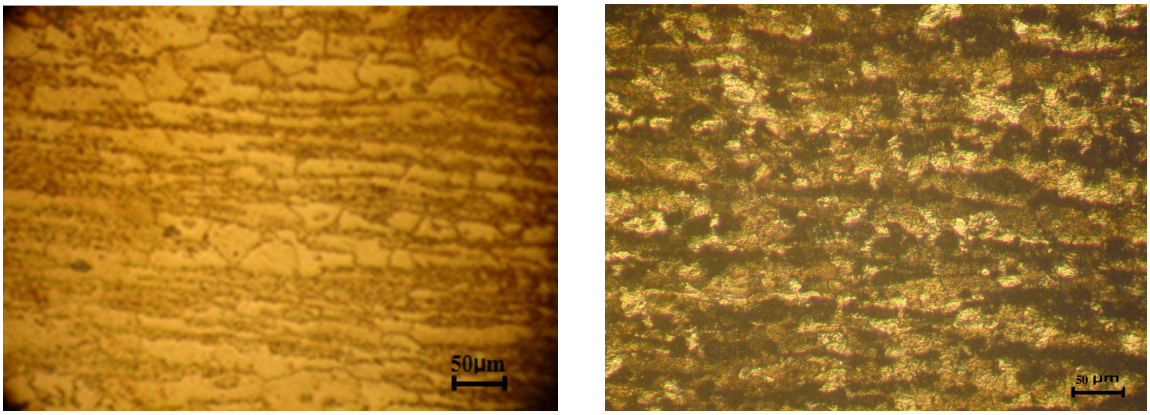

a) AISI 430 Stainless Steel b) Low Carbon steel AISI

Fig.3. Microstructures of base metals a) AISI 430 Ferritic stainless steel b) AISI 1020 Low Carbon steel

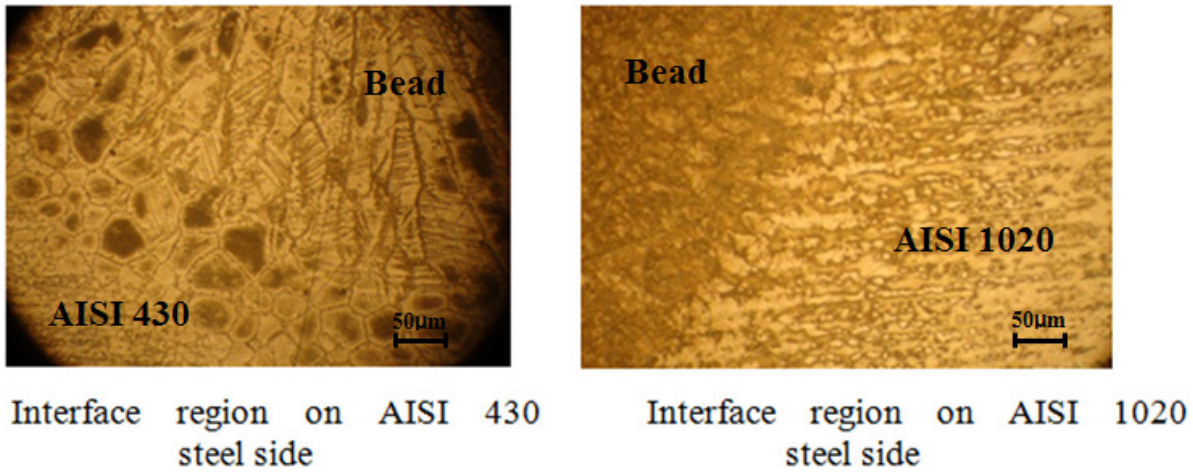

Fig. 4. Microstructures of dissimilar EB welded joint of AISI 430 ferritic stainless steel and AISI 1020 low carbon steel elaborated with I_w=24 mA, I_f=875 mA and v=8mm/s, at different zones.

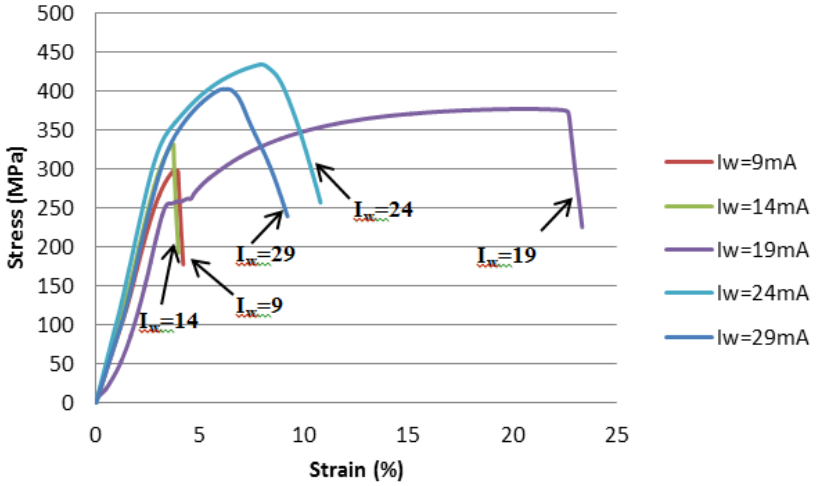

Fig. 5. Typical Stress-Strain curves obtained during testing welded dissimilar joints of ferritic stainless steel and low carbon steel, by different Iw with constant If=875 mA and v=8mm/s.

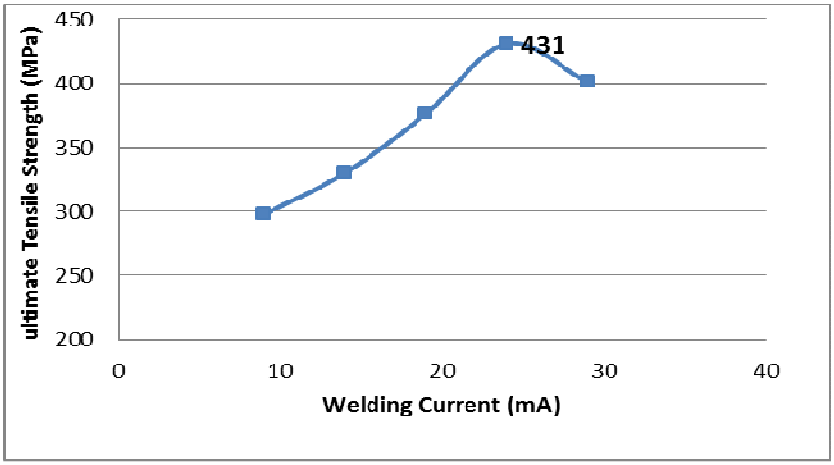

Fig. 6. The variation of the ultimate tensile strength obtained during tensile tests carried out on the dissimilar joints of AISI 430 ferritic stainless steel and AISI 1020 low carbon steel as a function of welding current and under constant If=875 mA and v=8mm/s.

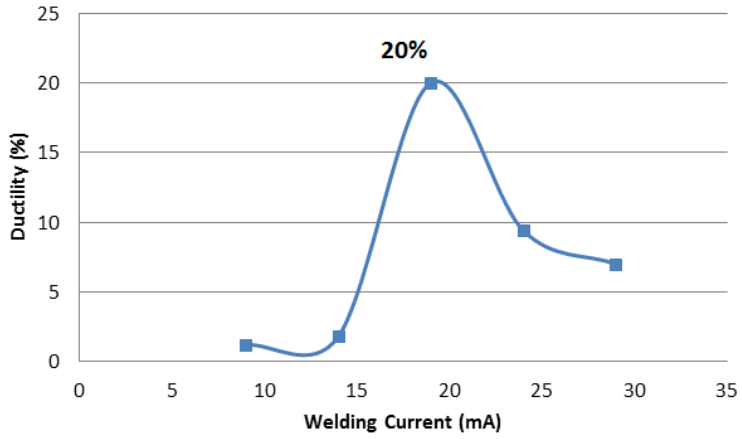

Fig. 7. The Variation of the ductility obtained during tensile tests carried out on the dissimilar joints of AISI 430 ferritic stainless steel and AISI 1020 low carbon steel as a function of welding current and under constant If=875 mA and v=8mm/s.

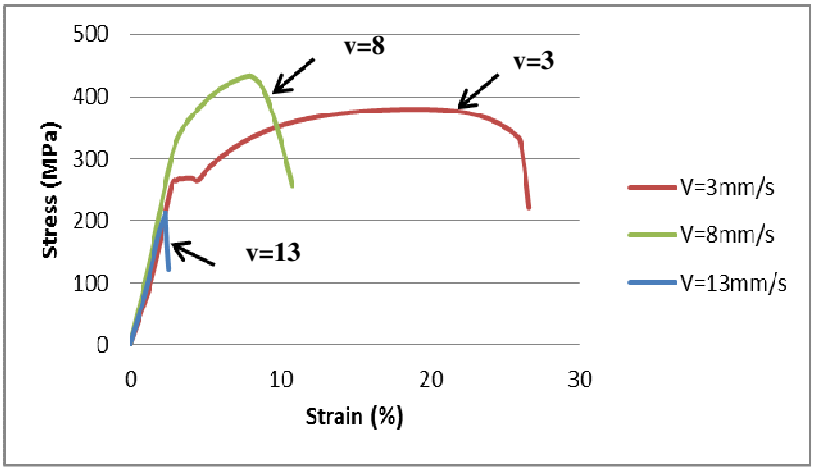

Fig. 8. Typical Stress-Strain curves obtained during testing welded dissimilar joints of ferritic stainless steel and low carbon steel, by different welding speed with constant Iw=24 mA and If=875 mA.

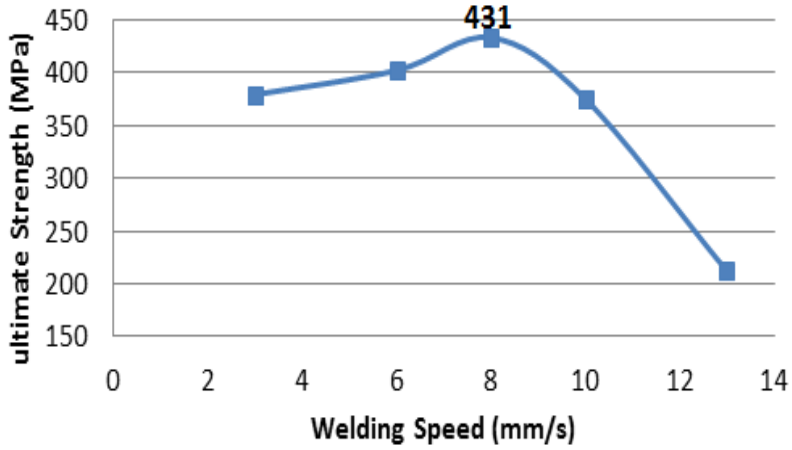

Fig. 9. The variation of the ultimate tensile strength against welding speed with constant Iw=24 mA and If=875 mA.

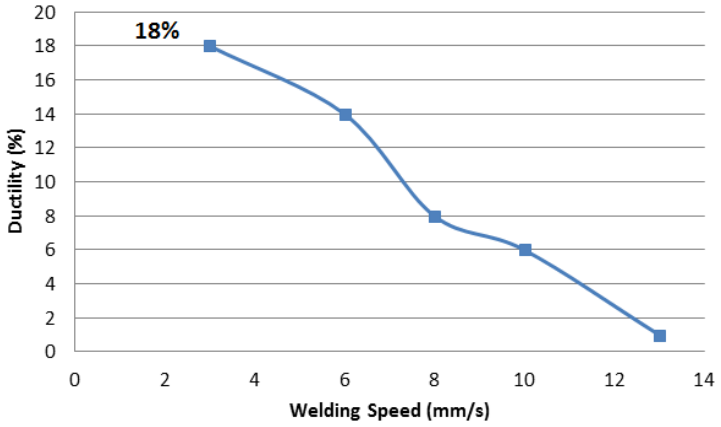

Fig. 10. The variation of the ductility of the joint against welding speed with constant Iw=24 mA and If=875 mA.

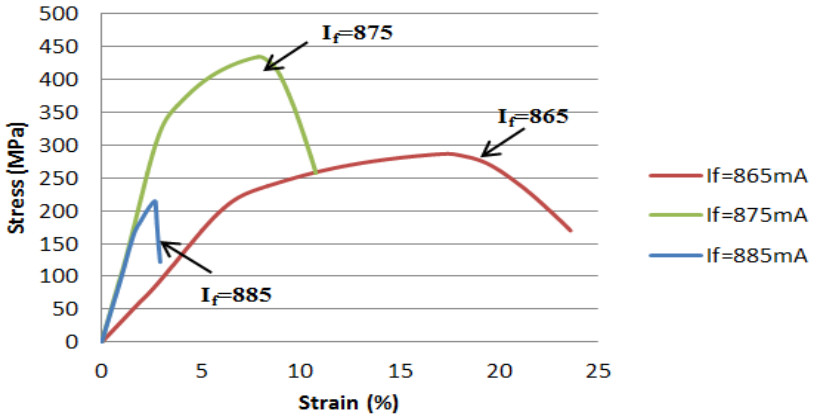

Fig. 11. Typical Stress-Strain curves obtained during testing welded dissimilar joints of austenitic stainless steel and low carbon steel, by different focusing current with constant Iw=24 mA and v=8 mm/s.

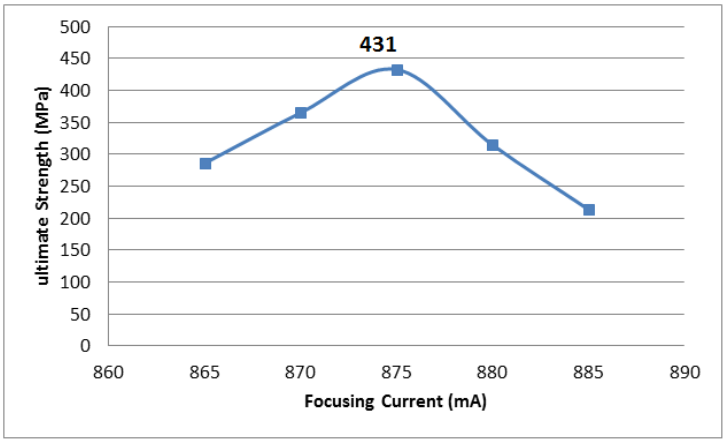

Fig. 12. The variation of the ultimate tensile strength against focusing current with constant Iw=24 mA and v=8 mm/s.

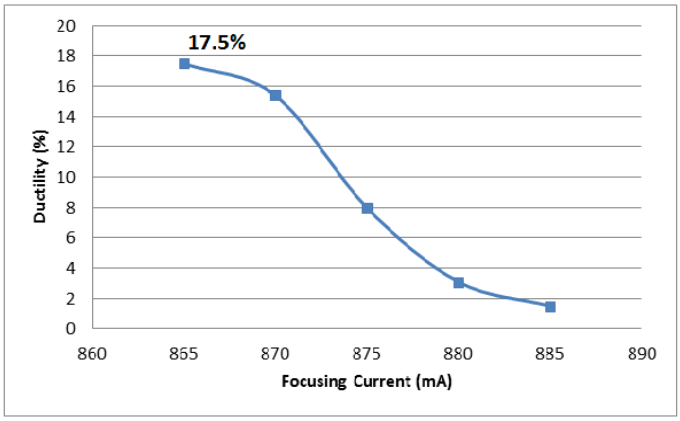

Fig. 13. The variation of the ductility of the joint against focusing current with constant Iw=24 mA and v=8 mm/s.

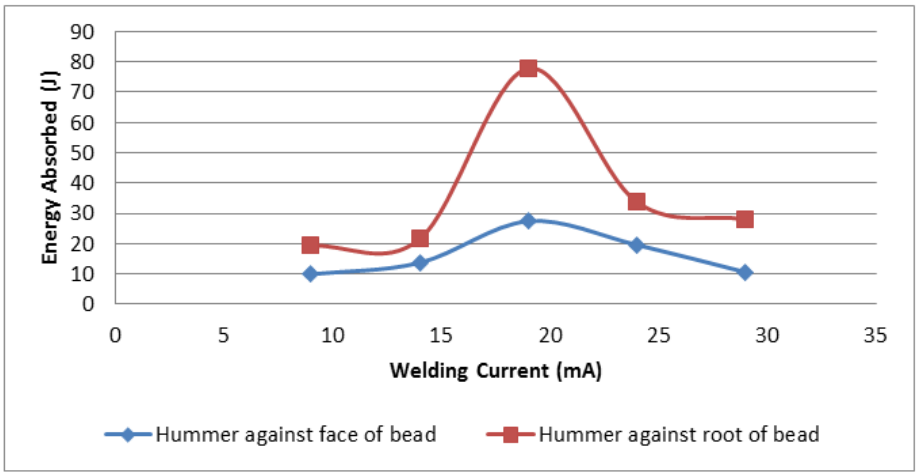

Fig. 14. The Effect of welding current on impact toughness, of welded dissimilar joints of ferritic stainless steel and low carbon steel, in the direction hammer against the face of bead, and in the opposite direction, hammer against the root of bead with constant If=875 mA and v=8 mm/s.

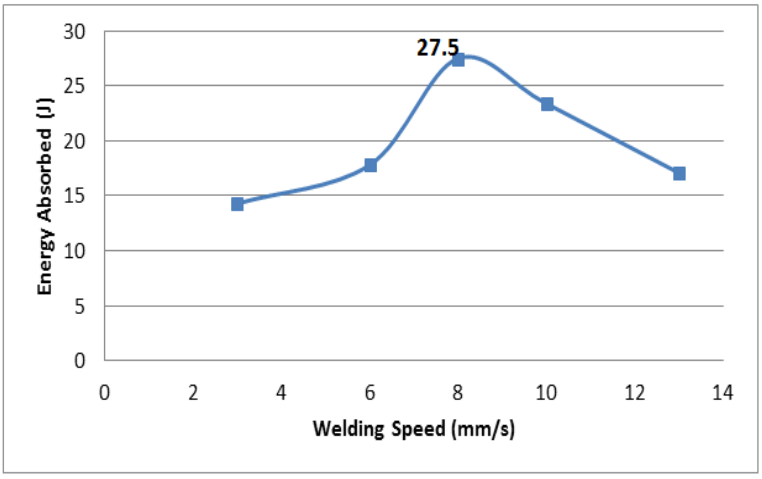

Fig. 15. The effect of welding speed on Impact Resistance, of welded dissimilar joints of ferritic stainless steel and low carbon steel at a constant optimum welding current of Iw=24 mA.

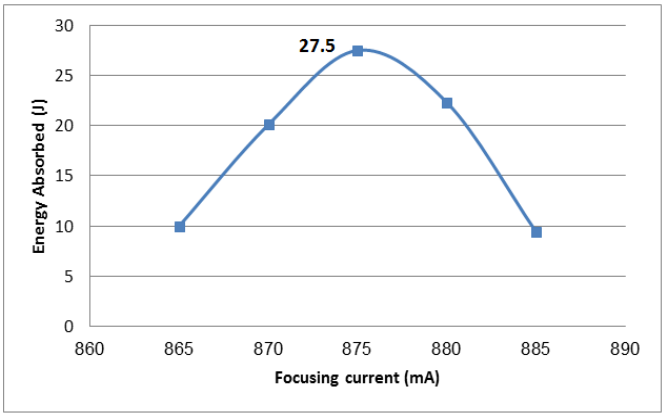

Fig. 16. The effect of focusing current on Impact Resistance, of welded dissimilar joints of ferritic stainless steel and low carbon steel at a constant optimum welding current of Iw=24 mA.

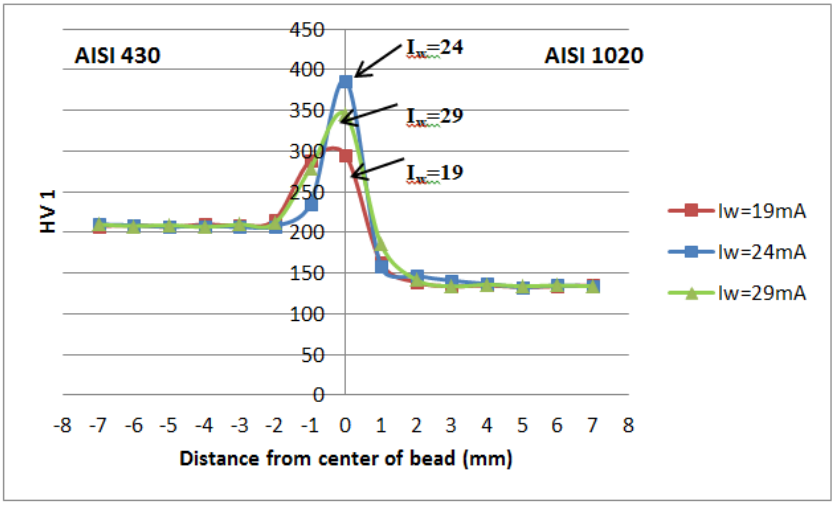

Fig.17. The hardness distribution, along a line, from the stainless steel side of the welded plates, through the heat affected zones and formed bead, to the low carbon steel side of the joint under different welding current and constant If=875mA, and v=8mm/s

Table 1. Chemical composition of base metals.

	C%	Mn%	Si%	Cr%	Ni%	Cu%	P%	S%	Fe%
AISI 430	0.12	0.37	0.9	15.8	0.18	0.023	0.04	0.03	balance
AISI 1020	0.21	0.45	0.25	0.019	0.025	0.013	<0.040	<0.050	balance